Enhanced reverse time migration of walkaway VSP data

Jing Wang* and Kristopher A. Innanen
jing.wang8@ucalgary.ca

Abstract

Elastic wave reverse time migration is a vector wave theory-based migration algorithm. Wavefields separation is an important step to remove crosstalk artifacts and improve imaging quality. Test results illustrate that the amplitude and phase of separated wavefields are changed and the polarity is reversed with Helmholtz decomposition, so that further correction are needed. Aiming to handle these, decoupled elastic wave equations are utilized to simulate the elastic wave propagation, which can maintain the vector property of original wavefields and give an ideal imaging profile without polarity reversal. With the separated vector wavefields, we implement a modified dot-product imaging condition for elastic RTM. Test on several numerical examples ademonstrate its feasibility and robustness for imaging complex subsurface structures. IIn this report, we firstly review the Helmholtz decomposition and analyze its shortcomings. Next, we utilize the decoupled elastic wave equations to obtain vector P- and S-wavefields with the same phases and amplitudes as the input coupled wavefields. And then, a dot-product imaging condition and corresponding elastic reverse time migration workflow are presented to produce PP- and PS-images. Finally, several numerical examples are used to illustrate the performance of this wavefield decomposition strategy and the corresponding workflow. Besides, the numerical simulation methods for the forward and backward wavefields' extrapolation, the effects of the multiples are also discussed in this report to further improve the imaging efficiency and accuracy.

Method

Helmholtz decomposition-based vector wavefield separation
At every time step of each wavefield extrapolation, the forward and backward multidimensional Fourier transforms had to be calculated, which is very expensive. Polarity is reversed.
Decoupled elastic wave equations-based elastic RTM
Vector P- and S-wavefields with the same phases and amplitudes as the input coupled wavefields are obtained.

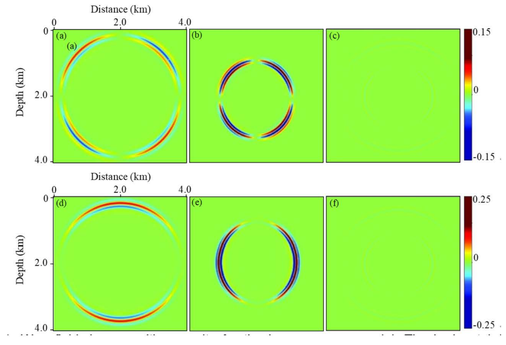

Figure: Wavefields decomposition results of horizontal (up) and vertical (down) components of P wavefield, S wavefield, and errors between the input and reconstructed wavefields. The reconstructed wavefields are computed by summing the decomposed P- and S-wavefields

A dot-product imaging condition (DP IMC) for vector-based elastic RTM
We retain the signs of the dot product and recompute the amplitudes using the multiplication of the absolute values of the separated source and receiver wavefields.

$$I^{\mathrm{PS}}(x,y,z)=\frac{\sum_t sign^{\mathrm{PS}}\cdot\left[\left|\mathbf{v}_{\mathbf{p}}^{\mathbf{src}}(x,y,z,t)\right|\cdot\left|\mathbf{v}_{\mathbf{s}}^{\mathbf{rcv}}(x,y,z,t)\right|\right]}{\sum_t\left[v_p^{src}(x,y,z,t)\cdot v_p^{src}(x,y,z,t)\right]},$$

$$sign^{\mathrm{PS}}=\mathrm{sign}\left[\mathbf{v}_{\mathbf{p}}^{\mathbf{src}}(x,y,z,t)\cdot\mathbf{v}_{\mathbf{s}}^{\mathbf{rcv}}(x,y,z,t)\right].$$

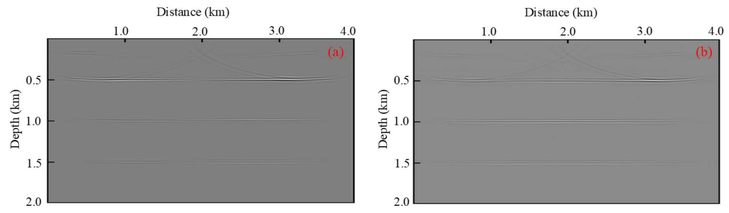

Figure: Polarity correction test for layers model. (a) no polarity correction, (b) polarity correction.

Numerical test results

In this section, we adopt the Marmousi model to illustrate the performance of the different elastic RTM methods.

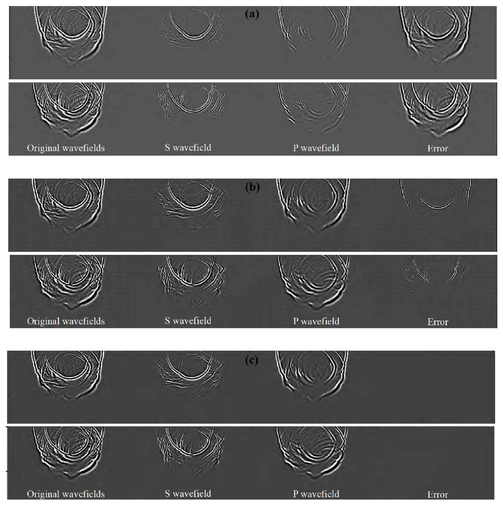

Figure: The horizontal (up) and vertical (down) components of wavefields decomposition. (a) Helmholtz decomposition, (b) Helmholtz decomposition with polarity correction, (c) Decoupled elastic wave equations

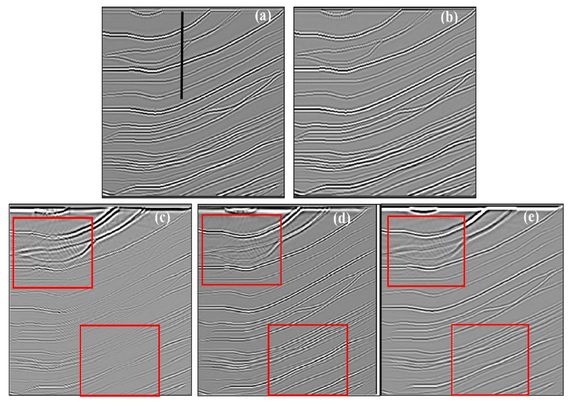

Figure: Images of the Maomousi truncation model. PP imaging with (a) Helmholtz decomposition, (b) Decoupled elastic wave equation; PS imaging with (c) Helmholtz decomposition, (d) Polarity correction-based Helmholtz decomposition, (e) Decoupled elastic wave equation

Conclusions

In order to improve the imaging quality and efficiency, we have made a lot of attempts, fucusing on the numerical simulation of wavefields extrapolation and separation, imaging condition, multiples, et al. Test on different synthetic models demonstrates the effects and imaging performance of these methods. In further works, we will further exploring the application of these aspects for field walkway VSP data.

Discussions

Variable length temporal and spatial operator finite difference method

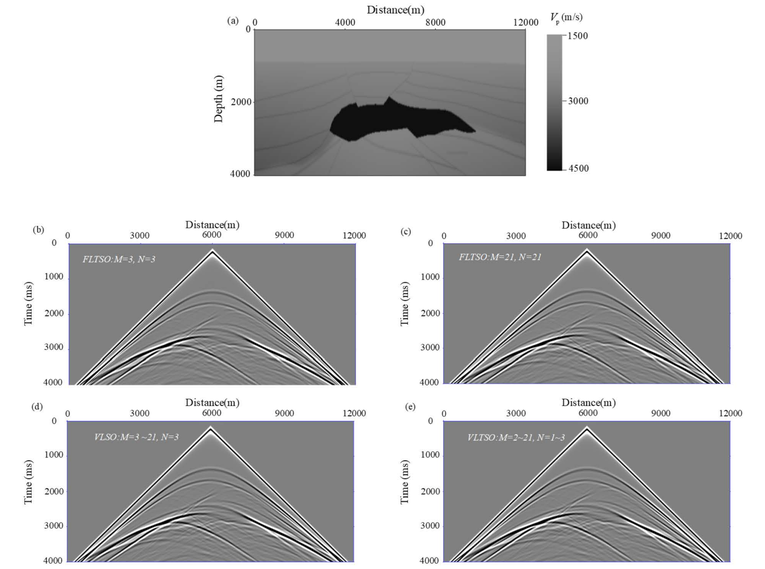

Figure: (a) 2D salt model. Seismic records of 4000 ms computed by (b) FLTSO with M=N=3, (c) FLTSO with M=N=21, (d) VLSO with N=3, M ranges from 3 to 21, (e) VLTSO with N ranges from 1 to 3, M ranges from 2 to 21 respectively

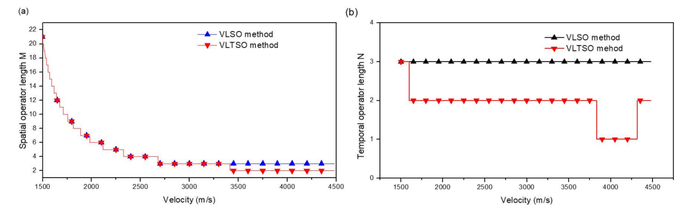

Figure: The spatial operator length M and temporal operator length N of VLSO and VLTSO methods

Table: CPU time comparison of the salt 2D modeling

Methods for 4000 ms simulation	CPU time (s)
FLTSO (M=N=21)	337.279
VLSO (N=3, M=3~21)	56.744
VLTSO (N=1~3,M=2~21)	53.951

Primaries and first-order multiples combination-based RTM

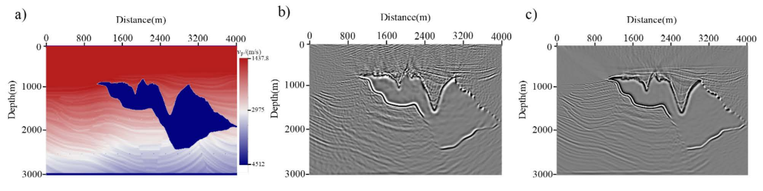

Figure: (a) Sigsbee 2B velocity model, (b) Primaries-based RTM image, (c)Primaries and first-order multiples combination-based RTM image

Acknowledgements

We thank the sponsors of CREWES for continued support. This work was funded by CREWES industrial sponsors and NSERC (Natural Science and Engineering Research Council of Canada) through the grant CRDPJ 543578-19.

NSERC CRSNG
UNIVERSITY OF CALGARY
FACULTY OF SCIENCE
Department of Geoscience